Monitoring of atmospheric ozone and nitrogen dioxide over the south of Portugal by ground-based and satellite observations

Daniele Bortoli[1, 3,*], Ana Maria Silva[1, 2], Maria João Costa[1, 2], Ana Filipa Domingues[1] and Giorgio Giovanelli[3]

[1]*Évora Geophysics Centre (CGE), University of Évora, Rua Romão Ramalho 59, 7000 Évora, Portugal;*
[2] *Department of Physics, University of Évora, Rua Romão Ramalho 59, 7000 Évora, Portugal;*
[3] *Institute of Atmospheric Sciences and Climate (ISAC-CNR), Via Gobetti 101, 40129 Bologna, Italy;*
*d.bortoli@isac.cnr.it

Abstract: The SPATRAM (Spectrometer for Atmospheric TRAcers Monitoring) instrument has been developed as a result of the collaboration between CGE-UE, ISAC-CNR and Italian National Agency for New Technologies, Energy and the Environment (ENEA). SPATRAM is a multi-purpose UV-Vis-scanning spectrometer (250 – 950 nm) and it is installed at the Observatory of the CGE, in Evora, since April 2004. A brief description of the instrument is given, highlighting the technological innovations with respect to the previous version of similar equipment. The need for such measurements automatically taken on a routine basis in south-western European regions, specifically in Portugal, has encouraged the development and installation of the equipment and constitutes a major driving force for the present work. The main features and some improvements introduced in the DOAS (Differential Optical Absorption Spectroscopy) algorithms are discussed. The results obtained applying DOAS methodology to the SPATRAM spectrometer measurements of diffused spectral sky radiation are presented in terms of diurnal and seasonal variations of nitrogen dioxide (NO_2) and ozone (O_3). NO_2 confirms the typical seasonal cycle reaching the maximum of $(6.5 \pm 0.3) \times 10^{+15}$ molecules cm^{-2} for the sunset values (PM), during the summer season, and the minimum of $(1.55 \pm 0.07) \times 10^{+15}$ molecules cm^{-2} for the sunrise values (AM) in winter. O_3 presents the maximum total column of (433 ± 5) Dobson Unit (DU) in the spring season and the minimum of (284 ± 3) DU during the fall period. The huge daily variations of the O_3 total column during the spring season are analyzed and discussed. The ground-based results obtained for NO_2 and O_3 column contents are compared with data from satellite-borne equipment (GOME - Global Ozone Monitoring Experiment; SCIAMACHY - Scanning Imaging Absorption Spectrometer for Atmospheric CHartographY; TOMS - Total Ozone Monitoring Spectrometer) and it is shown that the two data sets are in good agreement. The correlation coefficient for the comparison of the ground-based/satellite data for O_3 is of 0.97.

OCIS codes: (280.0280) Remote sensing and sensors; (300.6190) Spectrometers; (010.1280) Atmospheric composition; (010.4950) Ozone

---

References and links

1. J. K. Angell, and J. Korshover, "Global variation in total ozone and layer mean ozone: an update through 1981," J. Clim. Appl. Meteorol. **22**(9), 1611–1627 (1983).
2. R. Bojkov, and V. E. Fioletov, "Estimating the global ozone characteristics during the last 30 years," J. Geophys. Res. **100**(D8), 16537–16551 (1995).

3. W. C. Wang, Y.-C. Zhuang, and R. D. Bojkov, "Climate implication of observed changes in ozone vertical distribution at middle and high latitudes in the northern hemisphere," Geophys. Res. Lett. **20**(15), 1567–1570 (1993).
4. W. J. Randel, R. S. Stolarski, D. M. Cunnold, J. A. Logan, M. J. Newchurch, and J. M. Zawodny, "Trends in the vertical distribution of ozone," Science **285**(5434), 1689–1692 (1999).
5. Y. J. Orsolini, H. Eskes, G. Hansen, U. P. Hoppe, A. Kylling, E. Kyrö, and J. Notholt, "R. van der A and P. von der Gathen, "Summertime low-ozone episodes at northern high latitudes," Q. J. R. Meteorol. Soc. **129**, 3256–3275 (2003).
6. S. Solomon, and R. Garcia, "On the distribution of Nitrogen Dioxide in the High latitude stratosphere," J. Geophys. Res. **88**(C9), 5229–5239 (1983).
7. J. F. Noxon, E. C. Whipple, and R. S. Hyde, "Stratospheric NO_2 1. Observational Method and behaviour at mid latitude," Geophys. Res. Lett. **84**, 5047–5065 (1979).
8. F. Evangelisti, A. Baroncelli, P. Bonasoni, G. Giovanelli, and F. Ravegnani, "Differential optical absorption spectrometer for measurement of tropospheric pollutants," Appl. Opt. **34**(15), 2737–2744 (1995).
9. D. Bortoli, G. Giovanelli, F. Ravegnani, I. Kostadinov, and A. Petritoli, "Stratospheric Nitrogen Dioxide in the Antarctic," Int. J. Remote Sens. **26**(16), 3395–3412 (2005).
10. D. Hofmann, P. Bonasoni, M. de Maziere, F. Evangelisti, G. Giovanelli, A. Goldman, F. Goutail, J. Harder, R. Jakoubek, P. Johnston, J. Kerr, T. Mcelroy, R. Mckenzie, G. Mount, U. Platt, J. P. Pommereau, A. Sarkissian, P. Simon, S. Solomon, J. Stutz, A. Thomas, M. van Roozendael, and E. Wu, "Intercomparison of UV/Visible spectrometers for measurements of stratospheric NO_2 for the network for the detection of stratospheric changes," J. Geophys. Res. **100**(D8), 16765–16791 (1995).
11. H. K. Roscoe, P. V. Johnston, M. van Roozendael, A. Richter, A. Sarkissian, J. Roscoe, K. E. Preston, J.-C. Lambert, C. Hermans, W. DeCuyper, S. Dzienus, T. Winterrath, J. Burrows, F. Goutail, J.-P. Pommereau, E. D'Almeida, J. Hottier, C. Coureul, R. Didier, I. Pundt, L. M. Bartlett, C. T. McElroy, J. E. Kerr, A. Elokhov, G. Giovanelli, F. Ravegnani, M. Premuda, I. Kostadinov, F. Erle, T. Wagner, K. Pfeilsticker, M. Kenntner, L. C. Marquard, M. Gil, O. Puentedura, M. Yela, D. W. Arlander, B. A. Kastad Hoiskar, C. W. Tellefsen, K. Karlsen Tornkvist, B. Heese, R. L. Jones, S. R. Aliwell, and R. A. Freshwater, "Slant columns measurements of O_3 and NO_2 during the NDSC intercomparison of zenith-sky UV-visible spectrometers in June 1996," J. Atmos. Chem. **32**(2), 281–314 (1999).
12. D. Bortoli, "SPATRAM – SPectrometer for Atmospheric Tracers Measurements, A prototype equipment for the monitoring of minor compounds of the Atmosphere, Ph.D. thesis, University of Evora (2005).
13. D. Bortoli, A. M. Silva, and G. Giovanelli, "A new multipurpose UV-Vis spectrometer for air quality monitoring and climatic studies," Int. J. Remote Sens. (to be published).
14. J. P. Burrows, M. Weber, M. Buchwitz, V. Rozanov, A. Ladstätter-Weißenmayer, A. Richter, R. de Beek, R. Hoogen, K. Bramstedt, K.-U. Eichmann, M. Eisinger, and D. Perner, "The Global Ozone Monitoring Experiment (GOME): Mission concept and first scientific results," J. Atmos. Sci. **56**(2), 151–175 (1999).
15. R. D. McPeters, A. J. Krueger, P. K. Bhartia, J. R. Herman, C. G. Wellemeyer, C. J. Seftor, G. Jaross, O. Torres, L. Moy, G. Labow, W. Byerly, S. L. Taylor, T. Swissler, and R. P. Cebula, *Earth Probe Total Ozone Mapping Spectrometer (TOMS) Data Products User's Guide* (NASA Technical Publication, Maryland, 1998).
16. S. Noel, M. W. Wuttke, J. Skupin, H. Bovensmann, J. P. Burrows, M. Gottwald, and E. Krieg, "The SCIAMACHY instrument on ENVISAT: first performance monitoring results," in *Proceedings of IEEE International Geosciences and Remote Sensing Symposium* **5** (Centre de Congrè Pierre Baudés, Toulouse,2003), pp. 3120–3122.
17. U. Platt, "Differential Optical Absorption Spectroscopy (DOAS)," in *Air Monitoring By Spectroscopic Techniques*, Sigrist, M. W, ed. (Wiley-IEEE, 1994), pp 27–84.
18. A. S. Elokhov, and A. N. Gruzdev, "Nitrogen Dioxide Column Content and Vertical Profile Measurements at the Zvenigorod Research Station," Izv., Atmos. Ocean. Phys. **46**, 763–777 (2000).
19. W. Press, B. Flannery, S. Teukolsky, and W. Vetterling, *Numerical Recipies - The Art of Scientific Computing*, (Cambridge University Press, Cambridge, 1986).
20. D. J. Fish, "Measurements of stratospheric composition using ultraviolet and visible spectroscopy," Ph. D. thesis, University of Cambridge (1994).
21. K. V. Chance, and R. J. D. Spurr, "Ring effect studies: Rayleigh scattering, including molecular parameters for rotational Raman scattering, and the Fraunhofer spectrum," Appl. Opt. **36**(21), 5224–5230 (1997).
22. I. Kostadinov, G. Giovanelli, F. Ravegnani, F. Evangelisti, P. Bonasoni, R. Werner, and U. Bonafè, "Polarization and Ring Effect Influences upon Stratospheric DOAS Measurements," Proc. SPIE **3106**, 74–83 (1997).
23. G. Vaughan, H. K. Roscoe, L. M. Bartlett, F. M. O'Connor, A. Sarkissian, M. Van Roozendael, J.-C. Lambert, P. C. Simon, K. Karlsen, B. A. K. Høiskar, D. J. Fish, R. L. Jones, R. A. Freshwater, J.-P. Pommereau, F. Goutail, S. B. Andersen, D. G. Drew, P. A. Hughes, D. Moore, J. Mellqvist, E. Hegels, T. Klupfel, F. Erle, K. Pfeilsticker, and U. Platt, "An intercomparison of ground-based UV-visible sensors of ozone and NO_2," J. Geophys. Res. **102**(D1 D1), 1411–1422 (1997).
24. A. Petritoli, G. Giovanelli, P. Bonasoni, T. Colombo, F. Evangelisti, U. Bonafe, and D. Bortoli, Iv. Kostadinov and F. Ravegnani, "Ground Based NO_2 and O_3 Analysis at Mt. Cimone Station during 1995-1996: a case study for spring 1995 NO_2 concentration profile, in Spectroscopic Atmospheric Monitoring Techniques," Proc. SPIE **3867**, 280–289 (1999).
25. D. V. Ionov, V. P. Sinyakov, and V. K. Semenov, "Validation of GOME (ERS-2) NO_2 vertical column data with ground-based measurements at Issyk-Kul (Kyrgyzstan)," Adv. Space Res. **37**(12), 2254–2260 (2006).

26. V. E. Fioletov, J. B. Kerr, D. I. Wardle, N. Krotkov, and J. R. Herman, "Comparison of Brewer ultraviolet irradiance measurements with total ozone mapping spectrometer satellite retrievals," Opt. Eng. **41**(12), 3051–3061 (2002).
27. M. L. Salby, and P. F. Callaghan, "Fluctuations of total ozone and their relationship to stratospheric air motions," J. Geophys. Res. **98**(D2), 2715–2727 (1993).
28. G. Nikulin, and A. Karpechko, "The mean meridional circulation and mid-latitude ozone buildup," Atmos. Chem. Phys. **5**, 3159–3172 (2005).
29. R. D. Bojkov, D. S. Balis, "Characteristics of episodes with extremely low ozone values in the northern middle latitudes 1957-2000," Ann. Geophys. **19**, 797–807 (2001).
30. G. Koch, H. Wernli, C. Schwierz, J. Staehelin, and T. Peter, "A composite study on the structure and formation of ozone miniholes and minihighs over central Europe," Geophys. Res. Lett. **32**(12), L12810 (2005).
31. I. Wohltmann, M. Rex, D. Brunner, and J. Mader, "Integrated equivalent latitude as a proxy for dynamical changes in ozone column," Geophys. Res. Lett. **32**(9), 3395–3412 (2005).
32. A. Galliani, A. M. Siani, N. J. Muthama, and S. Palmieri, "Synoptic-scale fluctuations of total ozone in the atmosphere," Ann. Geophys. **14**(10), 1044–1050 (1996).
33. M. Antón, M. L. Cancillo, A. Serrano, J. M. Vaquero, and J. A. García, "Ozone mini-hole over southwestern Spain during January 2004: Influence over ultraviolet radiation," Geophys. Res. Lett. **34**, L10808 (2007).
34. A. Poberovskii, A. Shashkin, D. V. Ionov, and Y. M. Timofeev, D. Ionov, Y. Timofeev, "NO_2 content variations near St. Petersburg as inferred from ground-based and satellite measurements of scattered solar radiation," Izv., Atmos. Ocean. Phys. **43**(4), 505–513 (2007).
35. K. E. Preston, D. J. Fish, H. K. Roscoe, and R. L. Jones, "Accurate Derivation of Total and Stratospheric Vertical Columns of NO_2 from Ground-Based Zenith-Sky Measurements," J. Atmos. Sci. **30**, 163–172 (1998).
36. R. McKenzie, P. V. Johnston, C. T. McElroy, J. B. Kerr, and S. Solomon, "Altitude distributions of stratospheric constituents from ground-based measurements at twilight," J. Geophys. Res. **96**(D8), 15499–15511 (1991).

1. Introduction

In the last forty years, the stratospheric ozone (O_3) in the Northern Hemisphere (NH) mid-latitudes has suffered a significant decrease. The analysis of results obtained from TOMS (Total Ozone Mapping Spectrometer) installed onboard the Nimbus 7 satellite, underlines the significant reduction of the O_3 total column also before the Pinatubo eruption. During the eighties, studies of O_3 profile temporal series in the NH show that the annual average of O_3 concentration has increased in the troposphere and decreased in the low stratosphere [1]. Other authors confirm these results [2,3], emphasizing that, in Southern Europe, the trend of O_3 loss per decade is higher than the one found in the United States, also considering areas at the same latitudes and with equal values of surface nitrogen oxides. On the other hand, comparisons of the results obtained for both hemispheres led to the conclusion that O_3 loss is smaller at northern polar latitudes than the Antarctic depletion phenomena. At mid-latitudes, the O_3 loss is similar in both hemispheres, with values between 5% and 8% per decade [4]. Nevertheless, the physical processes that can justify these losses in the O_3 budget of the north mid-latitude are not completely explained. The hypothesis of the air mass transport from the polar vortex towards lower latitudes cannot be completely applied to the NH. In fact, Arctic regions show very different meteorological conditions as higher average temperatures that do not favor Polar Stratospheric Cloud (PSC) formation. On the other hand, the lower polar vortex strength allows for losing its shape causing air mass intrusions that may reach the mid-latitudes. Moreover, the decrease of stratospheric O_3 during summer time at northern high latitudes is caused by chemical reactions and transport processes [5].

For some years the nitrogen compounds were thought to be most responsible for the ozone catalytic destruction. The understanding of the dynamical processes and chemical and photochemical reactions involving nitrogen compounds in the stratosphere has improved in the last years. The existence of a winter drop in nitrogen dioxide (NO_2) total column at high latitudes has been explained by the coupling of dynamical and chemical phenomena [6]. As clearly shown by Noxon [7], the horizontal meridional transport plays a very important role at mid-latitudes: air can move very rapidly from the high to the low latitudes, depending on the weather conditions. Sometimes this process of dislocation is slow so the chemistry of NO, NO_2, N_2O_5 and HNO_3 can play the primary role in the nitrogen compounds' partitioning, following the change in temperature and in daylight hours. From the chemical point of view, NO_2 can be oxidized by O_3 to form nitrate (NO_3), a strong atmospheric oxidant and a precursor to the formation of dinitrogen pentoxide (N_2O_5). Because NO_3 is rapidly photolyzed

at visible wavelengths, both its daytime concentration and chemistry are of relatively minor importance in the lower and middle stratosphere. In contrast, N_2O_5 can have morning concentrations in the lower stratosphere comparable to NO_x ($NO + NO_2$) even though its production requires the formation of NO_3.

$$NO_2 + O_3 \quad \rightarrow NO_3 + O_2 \tag{1}$$

$$NO_3 + h\nu \quad \xrightarrow[(\sim 90\%)]{\lambda < 580nm} NO + O_2 \tag{2}$$

$$NO_3 + h\nu \quad \xrightarrow[(\sim 10\%)]{\lambda < 640nm} NO_2 + O \tag{3}$$

$$NO_3 + NO_2 + M \rightarrow \quad N_2O_5 + M \tag{4}$$

$$N_2O_5 + h\nu \quad \rightarrow NO_3 + NO_2 \tag{5}$$
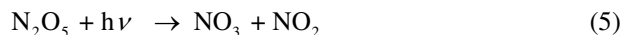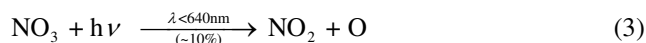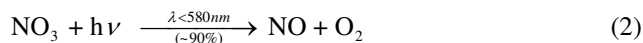
During the night N_2O_5 builds up, at the expense of NO, or more precisely of NO_2 (Eq. (4). After sunrise, N_2O_5 can be photolyzed giving rise to two NO_x molecules (Eq. (5); the photolysis time constant is dependent on both the usual factors (zenith angle, altitude, albedo, etc.) and the temperature.

To understand these stratospheric chemical reactions both satellites and the ground-based spectrometers played a key role by capturing major stratospheric features. Ground-based stations have been providing for many years a large amount of useful measurements to study atmospheric chemistry and dynamics and to monitor environmental pollution. From such stations, a long-term data set was built up in many regions of the planet to study the time variations of stratospheric trace gases, aerosol loading and other important physical parameters.

This study presents trace-gas vertical column results obtained from DOAS (Differential Optical Absorption Spectroscopy) methodology applied to the diffused spectral sky radiation measured along the zenith direction with the SPATRAM (SPectrometer for Atmospheric Tracers Measurements) instrument, developed by the Atmospheric Physics and Climate group of the Geophysics Centre of the University of Evora (CGE-UE) in close collaboration with the ISAC-CNR located in Bologna-Italia and with ENEA (Italian National Agency for New Technology, Energy and Environment). The instrument is installed at the observatory of the CGE-UE – south of Portugal (38.56°N, 7.91°W, 300m asl) since April 2004. The main features of this ground-based equipment are summarized in section 2. Section 3 gives a brief description of the satellite instruments from which data are used for comparison with SPATRAM results, namely the GOME - Global Ozone Monitoring Experiment, TOMS - Total Ozone Mapping Spectrometer and SCIAMACHY - Scanning Imaging Absorption Spectrometer for Atmospheric CHartographY. Subsequently, this study presents in Section 4 the methodology to obtain the total column content of atmospheric trace gases, namely of NO_2 and O_3 compounds, from the spectral irradiances, measured with SPATRAM, along the zenith direction. Section 5 presents and discusses the results obtained with the ozone column content and the comparison with equivalent results of NO_2 and O_3 total column contents obtained from satellite-borne equipment. Finally, section 6 summarizes the main conclusions and points out some directions for progress.

2. Ground - based Instrument

The SPATRAM is a multi purpose UV-Vis spectrometer for measurements of radiation in the spectral range from 250 to 950 nm. The equipment is based on the optical module of its progenitor the "old" GASCOD spectrometer [8,9]. GASCOD stands for Gas Analyzer Spectrometer Correlating Optical Differences and it was developed at the ISAC-CNR Institute (formerly FISBAT) during '93-'94. It has been tested in two NDSC (Network for the Detection of the Stratospheric Changes) campaigns [10,11].

In the SPATRAM, the spectrometer is installed inside a thermostatic box able to keep the internal temperature within the working range of the instrument (typically 15°C for the

Optical Unit). The equipment (Fig. 1) allows for multiple input of the radiation: i) from the primary input that is composed of a pair of flat and spherical mirrors that focus the light beam on the entrance slit (0.1 × 8 mm); ii) from the two lateral inputs, where the signal is carried to the entrance slit with an optical fiber connected to a very simple optical system, and iii) an additional input for spectral and radiometric calibration. A rotating mirror, driven by a stepper motor, allows for choosing between the primary input (pointing to the vertical), the optical fiber ones and the additional input for spectral or radiometric calibration.
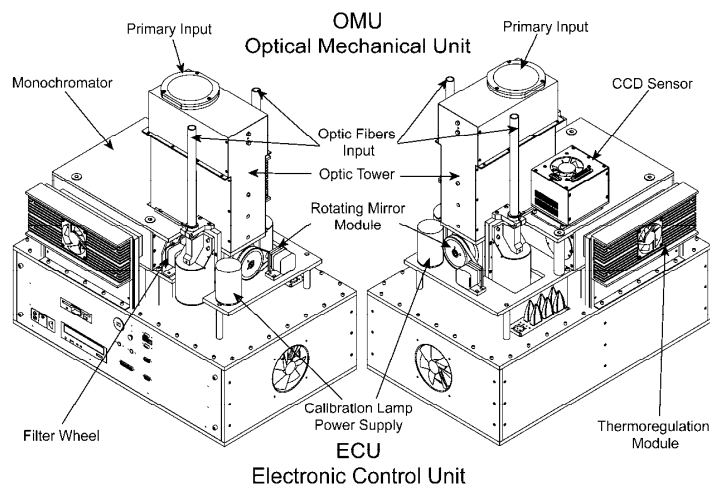
Fig. 1. Illustration of the SPATRAM instrument from 2 different points of view, allowing for the identification of its main modules

The spectrometer is composed of the holographic spherical diffraction grating of 1200 grooves/mm and a Back Illuminated CCD (Charge Coupled Device) sensor array manufactured by *'e2v – space and scientific sensors'* and customized for our purposes in terms of cooling capability and AD signal conversion. The CCD sensor is composed of 1024 × 254 pixels over the length of 1 inch and each pixel has the dimension of 24 μm, giving a full dimension of 25.4 × 6.6 mm. The CCDs have a big quantum efficiency allowing to perform the so-called 'binning' of the vertical pixels in order to obtain high sensitivity (therefore short exposure times) and high Signal to Noise Ratio (SNR) in the measurements. In order to minimize the effects on the measurements of the dark and read current, one double stadium Peltier circuit cools the CCD chip till –40°C. The grating is controlled by a stepper motor which, by varying the angle of incidence of light, allows the instrument to obtain measurements from 250 to 950 nm in spectral windows of 60 nm each. The spectral dispersion is approximately 2.4 nm/mm (depending on the investigated spectral region), and the overall typical spectral resolution is about 0.5 nm. Band-pass filters are used to remove the interferences caused by the different order of dispersion and to reduce the stray light inside the spectrometer. The integration time is automatically selected for each reading and ranges from tenths of milliseconds at noon to tenths of seconds at twilight. An internal mercury lamp is used for periodic checks of the diffraction grating positions, ensuring a spectral accuracy better than 0.05 nm. The Electronic Control Unit (ECU) (rigidly connected to the Optical Mechanical Unit - OMU) contains an industrial monoboard (NOVA7892), equipped with 1 GHz CPU and 512 MB of RAM, a CCD driver device, the 3 controllers for the stepper motors, an AD converter for the temperature transducers, present in both units OMU and ECU and other electric and electronic components for the full management of the instrument. The SPATRAM is handled by a software tool (DAS – Data Acquisition System) that was also developed by the first author, in order to control the spectrometer devices and

for automatic scheduled measurements; the ECU provides also the storage of the measured spectral data as well as the pre-processing of the data and of their first analysis, with DOAS methodology. SPATRAM can provide the column content of all the compounds presenting absorption features in the investigated spectral range. The standard products that have been obtained are O_3 and NO_2 in the UV and Visible spectral region respectively (specifically 320-340 nm for O_3 and 430-450 nm for NO_2). In the near future also the column content of other species, such as SO_2, BrO, H_2CO will be included in the retrieval. The SPATRAM instrument allows for the retrieval of the minor compounds in the atmosphere, with improved temporal resolution, flexible management and enhanced capability of measurements with respect to the GASCOD spectrometer. A full description of the instrument, of the novelty of the equipment in relation to GASCOD can be found in [12,13].

3. Satellite data source

At the end of the seventies, the satellite instruments started to provide very useful information regarding the status of our atmosphere and the variation of its compounds. In the last 10 years, the number of satellite instruments monitoring atmospheric trace gases has increased considerably. Ground-based instruments can provide long and stable data records for a specified location. On the other hand, satellite instruments are the most effective way to accomplish a global view of the atmosphere, but they have to be continuously validated to guarantee the ongoing quality of the measured data and to avoid long-term drifts in their data by instrumental aging effects. A short presentation of the space-borne sensors used in the present work is given in this section.

3.1 GOME – Global Ozone Monitoring Experiment

The European Remote Sensing satellite (ERS-2) was launched in April 1995 into a near-polar sun-synchronous orbit at a mean altitude of 795 km. The descending node crosses the equator every 2800 km at 10:30 local time. GOME, on board ERS-2 satellite, is a nadir-scanning double monochromator covering the 237 nm to 794 nm wavelength range with a spectral resolution of 0.17-0.33 nm. The spectrum is split into four spectral channels, each recorded quasi-simultaneously by a 1024-pixel photodiode array. The global spatial coverage of the Earth is obtained within 3 days at the equator by a 960 km across-track swath (4.5 s forward scan, 1.5 s back scan). The ground pixel size of the measurements is 320×40 km^2. The down welling solar irradiance is also measured by the GOME sensor. By means of DOAS methodology, GOME provides the total column of O_3 as well as of NO_2 and other tracers such as SO_2 and formaldehyde (H_2CO). Details of the overall scientific objectives of GOME and instrument concept are reported in [14].

3.2 TOMS – Total Ozone Monitoring Spectrometer

The Nimbus 7 spacecraft was in a south-to-north, sun-synchronous polar orbit so that it was always close to local noon/midnight below the spacecraft. Thus, ozone measurements are taken for the entire Earth every 24 hours. TOMS, on board the Nimbus 7 satellite, directly measures the ultraviolet sunlight scattered by the Earth's atmosphere in six different 1-nm bands. Total column ozone is inferred from the differential absorption of scattered sunlight in the ultraviolet range by taking the ratio of two wavelengths (312 nm and 331 nm, for example), where radiation is strongly absorbed by ozone in one wavelength while absorption is only weakly in the other. The instrument has a 50 kilometers square field of view at the sub-satellite point. TOMS collects 35 measurements every 8 seconds as it scans right to left producing approximately $2 \times 10E + 5$ ozone measurements daily [15].

3.3 SCIAMACHY – Scanning Imaging Absorption Spectrometer for Atmospheric CHartographY

ENVISAT was launched in 2002 and it is the largest Earth Observation spacecraft ever built. It carries ten sophisticated optical and radar instruments to provide continuous observation

and monitoring of the Earth's land, atmosphere, oceans and ice caps. ENVISAT data collectively provide a wealth of information on the mechanisms of the Earth system, including insights into factors contributing to climate change. SCIAMACHY is one of the 10 instruments installed on board ENVISAT. SCIAMACHY is an imaging spectrometer whose primary mission objectives are measurements of trace gases in the troposphere and in the stratosphere. The solar radiation transmitted, backscattered and reflected from the atmosphere is recorded at relatively high resolution (0.2 nm to 1.5 nm) over the range 240 nm to 1700 nm, and in selected regions between 2.0 µm and 2.4 µm [16]. Since SCIAMACHY is the evolution of the GOME sensor in the UV-Vis spectral range (300-700 nm) the same tracers (O_3, NO_2, SO_2 and others) are retrieved by applying the DOAS algorithms, with an improved spatial resolution (typically the ground pixel is 30×240km.).

4. Methods

In order to obtain information on the performance of the SPATRAM instrument and the quality of the measured data, the "Flux Index" (FI), namely the ratio of the mean spectral signal obtained by the spectrometer during the measurement and the "exposure" time [9], is calculated. The FI provides information on the variation of the incoming radiation quantity; therefore the FI can be used for the first evaluation of the quality of the measured spectral data.
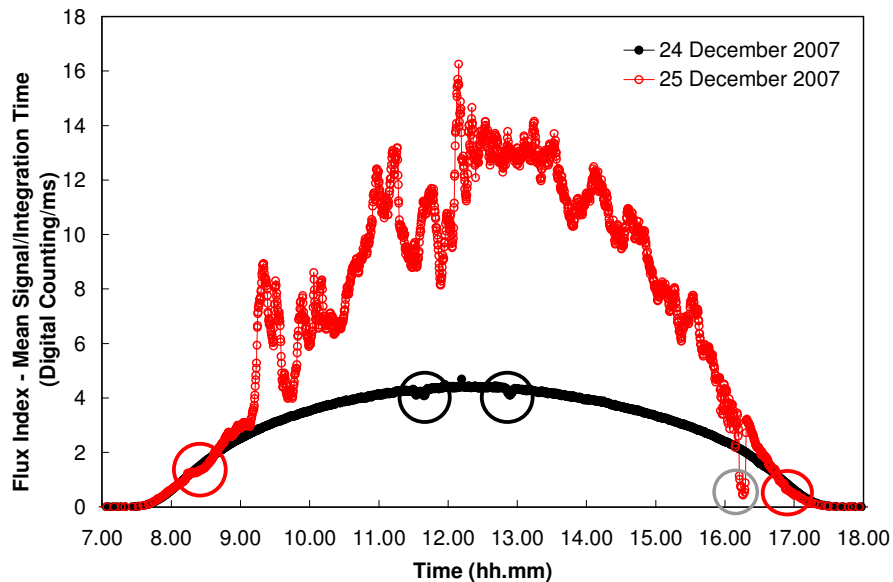

Fig. 2. Flux Index – FI – (ratio of the signal obtained by the spectrometer and its "exposure" time) calculated at the Evora station for 2 days under different meteorological conditions. The FI on 24 December 2007 - cloudless day – presents a regular behavior, while on 25 December 2007 - cloudy day – more scattered values of FI are obtained

Figure 2 shows the FI for two days under different meteorological conditions at the Evora station. The FI values describe a regular function (Fig. 2, black dots) during cloud-free days. In cloudy conditions, the FI can increase by up to 4 times (Fig. 2, open circle) mainly due to the increase of the multiple scattering produced by the presence of clouds. However, most of the measurements obtained with the SPATRAM are not affected by the increase in radiation flux, since the spectral measurements are carried out by applying the auto ranging mode in order to find the optimal integration time and, hence, achieve the highest SNR. The 'auto ranging' (*ar*) procedure is based on the linearity of the CCD charge with time: one measurement with the fixed exposure time of 100 ms is used for the determination of the

exposure time to be applied in the following measurement. The raw data obtained by the spectrometer are rejected and are not used in the DOAS processing if the corresponding value of FI is considerably lower than the regular function expected (case of cloud-free conditions). In fact, the integration time required to obtain the maximum signal established a priori could be greater than the maximum exposure time the instrument is capable of. On the other hand, the temporary obstruction of the spectrometer radiation input may lead to carry out measurements with a radiation flux lower than the one used in the *ar* algorithm for computation of the optimum exposure time. In Fig. 2, the analysis of the data concerning the cloudless day reveals 3 episodes of deviation from the expected behavior between 11:30 and 13:00. The positive variation with respect to the regular function, observed at 12:14, was caused by the increase in the multiple scattering due to a thin cloud entering the field of view (FOV) of SPATRAM, not significantly affecting the measurements, since the *ar* procedure takes into account the increase of the radiation flux for the determination of the exposure time. In contrast, clouds could move so fast that the boundary conditions during the *ar* and the measurement are changed. In this case the integration time would not be optimal for the highest SNR, leading to a lower signal than expected (black open circles in Fig. 2). These last measurements are still exploitable in the DOAS processing, even if particular attention has to be devoted during the analysis of results, considering the slightly low value of the FI. The FI plot for the cloudy day underlines 3 different situations: i) the slight deviation from the regular function occurring during the sunrise and sunset periods (red open circles in Fig. 2); ii) the scattered values of FI due to multiple scattering produced by clouds during almost the whole day, from 9:15 to 16:30; iii) the episode of very low FI values (light gray open circle in Fig. 2) taking place between 16:15 and 16:25, due to the presence of very thick clouds in the FOV of the instrument. Only for the last case, the spectral measurements are considered unreliable and thus not utilized in the DOAS processing.

A complete description of Differential Optical Absorption Spectroscopy (DOAS) can be found in several references [7,17,18]. Nevertheless, some aspects of the processing algorithm are discussed below.

In order to obtain the absorption structure of the gases under investigation, the Fraunhofer lines of the solar spectra should be removed. The logarithm of the ratio $Log\_Ratio(\lambda, \theta)$ between a reference spectrum ($I_o(\lambda, \theta_{Min})$) and the twilight spectrum ($I_s(\lambda, \theta)$), both measured with the SPATRAM, is calculated. θ is the Solar Zenith Angle (SZA) and θ_{Min} is reached at the local noon. The high-frequency features are removed by applying a low-pass filter operator to the $Log\_Ratio(\lambda, \theta)$ spectrum. The low pass filter operator is obtained with the Fast Fourier Transform algorithms [19] and here in after the over-striking notation is adopted to identify the filtered terms in the equations. The normalized difference between $Log\_Ratio(\lambda, \theta)$ and $\overline{Log\_Ratio(\lambda, \theta)}$ is referred to as the 'differential' spectrum (Eq. (6).

$$Log\left(\frac{I_o(\lambda,\theta)}{I_s(\lambda,\theta)}\right) - \overline{Log\left(\frac{I_o(\lambda,\theta)}{I_s(\lambda,\theta)}\right)} = \sum_g \Delta\sigma_g(\lambda)SCD_g(\theta) \qquad (6)$$

In Eq. (6) the filter operator is applied directly to the cross section of the absorber's ($\sigma_g(\lambda)$). The differential spectrum is compared with the differential absorption cross sections ($\Delta\sigma_g(\lambda) = \sigma_g(\lambda) - \overline{\sigma_g(\lambda)}$) of the atmospheric trace gases under investigation, which present measurable absorption features in the selected spectral range in order to retrieve the Slant Column Density ($SCD_g(\theta)$ – the number of molecules of the gth absorber per square centimeter, along the optical path of measure). In Fig. 3 the typical results of Eq. (6) for O_3 retrieval, are reported.
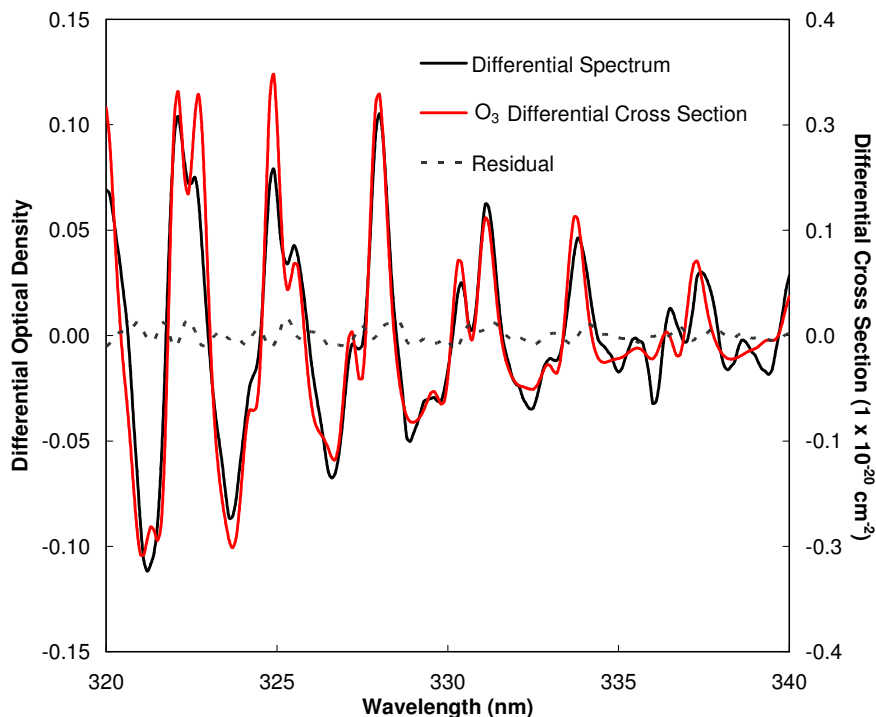
Fig. 3. The 'Differential' spectrum – black line – (the difference between Log_Ratio and Smooth (Log_Ratio), where Smooth(x) is a low pass filter operator) and the O_3 Differential Cross Section – red line – are plotted towards the left and right axis respectively. In the selected spectral range, the differential spectrum features show good agreement with the differential cross section ozone, allowing for the determination of its atmospheric content. In addition also the residual of the DOAS processing – gray line – is shown.

To achieve a perfect spectral alignment, the so-called 'shift' and 'stretch' procedures are used [20]. The solution of the Lambert Beer equation, in its differential form (the DOAS Master Equation – Eq. (6), is obtained by means of the Singular Value Decomposition (SVD). Marquardt's method [19] is used to minimize the Sum Of Squares (SOS) of the residual spectrum, using the derivative of the SOS function and modifying the shift and stretch functional parameters. Scattering processes and polarization effects can introduce systematic errors in the retrieved amounts. Therefore, additional 'non-absorption' cross sections such as Mie, Rayleigh, Ring and polarization are introduced [21,22].

In the retrieval of the $SCD_g(\theta)$ for the gth absorber, it has to be taken into account that $I_o(\lambda, \theta_{Min})$ is obtained at the local noon, when the absorption of minor compounds is small but not zero. Hence, the actual values retrieved from Eq. (6) are the Differential Slant Column Density ($DSCD_g(\theta)$), which is the difference between the gas content value derived from the $I_s(\lambda, \theta)$ and the gas content in $I_o(\lambda, \theta_{Min})$. In this regard, the problem of the absorber content determination in the reference spectrum ($SCD_{g,I_o}(\theta_{Min})$), arises [23].

For the estimation of the $SCD_{g,I_o}(\theta_{Min})$, the definition of the Air Mass Factor (AMF) has to be introduced as the ratio between the $SCD_g(\theta)$ and the Vertical Column Densities (VCD_g)

$$AMF_g(\theta, \lambda) = SCD_g(\theta) / VCD_g \qquad (7)$$

The AMF depends on wavelength as Rayleigh scattering is a strong function of wavelength, within the used UV-Vis spectral range and the absorption also varies with wavelength. At low sun, the AMF is smaller in the UV than in the visible as more light is scattered before traveling the long distance in the atmosphere. On the other hand, at high sun, the opposite is true as a result of multiple scattering.

In Bortoli [9], a method for the determination of $SCD_{NO_2,I_o}(\theta_{Min})$, is presented. The technique is based on some simple consideration regarding the steady concentrations of NO_2 at high latitudes during the summer period. At mid-latitudes, the Langley plots of the retrieved values during one day, before the local noon (AM) and after the local noon (PM) versus the series of the calculated AMF values are usually used to estimate the content of the analyzed compound in the reference spectrum. The evaluation of the $SCD_{g,I_o}(\theta_{Min})$ cannot be obtained by applying of the DOAS algorithms to the reference spectrum itself, since the associated system will be singular. The $SCD_g(\theta)$ can finally be calculated as follows:

$$SCD_g(\theta) = DSCD_g(\theta) + SCD_{g,I_o}(\theta_{Min}) \tag{8}$$

and the Vertical Column Density (VCD_g) of the investigated specie determined according to Eq. (7)

In this work, the spectrum measured with the SPATRAM instrument in the 405-465 nm spectral interval on 29 July 2004 at local noon was selected as reference spectrum for the retrieval of the $DSCD_{NO_2}(\theta)$. The choice is driven by analysis of diurnal variation of the FI values, allowing for identification of 29 July as a cloudless day, with very high sun elevation therefore with the minimum content of $SCD_{NO_2,I_o}(\theta_{Min})$.

In Fig. 4(a), it is shown that the AM $DSCD_{NO_2}(\theta)$ values are lower than the PM ones, as expected due to the NO_2 photochemical activity in reactions (1)-(5); this aspect leads to two fitting straight lines converging to the value of $SCD_{NO_2,Io}(\theta_{Min})$ at local noon, when $AMF = \cos(SZA)^{-1}$ is close to 1. Due to the greater errors mainly caused by the shorter optical path of measurements, the separate best fits of the AM and PM values do not intercept at the value of the minimum AMF of the day, providing two different values for the NO_2 content for AMF = 1 $(3.53 \pm 0.07) \times 10^{+15}$ and $(6.68 \pm 0.13) \times 10^{+15}$ molecules cm^{-2} for the AM and PM series respectively. Another approach consists in considering the AM and PM series together, in order to eliminate the effects due to possible spikes in the $DSCD_{NO_2}(\theta)$, in particular for the lowest values of AMF. After performing the latter computation, the red line in Fig. 4 is obtained and the $DSCD_{NO_2}(\theta)$, for the minimum AMF of the chosen day, lead to the value of $(4.98 \pm 0.10) \times 10^{+15}$ molecules cm^{-2}. This last value is considered as the NO_2 background content ($SCD_{NO_2,Io}(\theta_{Min})$) of the reference spectrum and has to be added to the retrieved $DSCD_{NO_2}(\theta)$ in order to have the SCD_{NO_2}, according to Eq. (8).

For the computation of the ozone amount in the reference spectrum, the $DSCD_{O_3}(\theta)$ values obtained for 3 April 2004 are plotted versus the calculated AMF as shown in Fig. 4(b). The photochemical rates of O_3 are almost 3 order of magnitude lower than the ones for the NO_2, therefore the usual diurnal variations of the O_3 total columns are not so significant as for NO_2, hence the AM and the PM values for ozone are almost overlapped and the linear fitting function of both series can be used in order to evaluate the ozone content in the reference spectrum. For AMF = 1 the value of $(2.49 \pm 0.05) \times 10^{+17}$ molecules cm^{-2} is obtained (9.2 Dobson Unit - DU). This value is considered as the background content of O_3 in the reference

spectrum ($SCD_{O_3,Io}(\theta_{Min})$) and it has been added to the retrieved $DSCD_{O_3}(\theta)$ values in order to have the SCD_{O_3} .
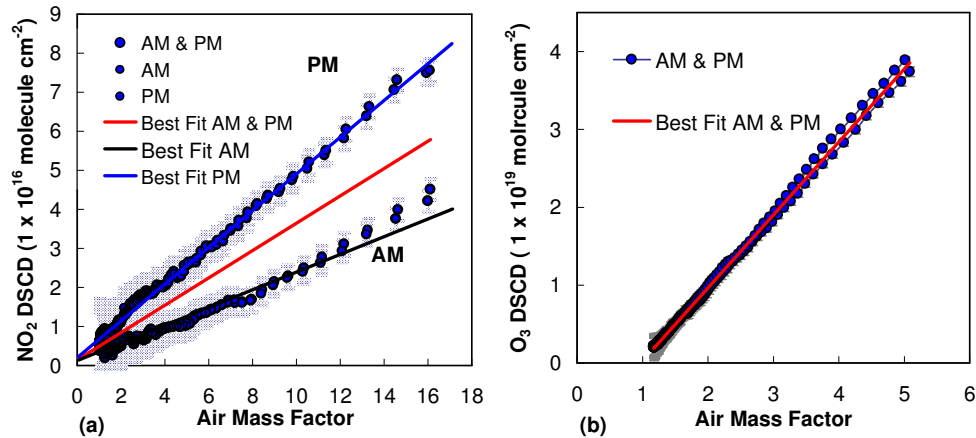

Fig. 4. (a) NO$_2$ DSCD AM and PM values, obtained for the 29 July 2004, plotted versus the calculated AMF. The best fits for the AM values (black line), PM values (blue line) and for both (red line) are shown; (b) O$_3$ DSCD AM and PM values, obtained for 3 April 2004, plotted versus the calculated AMF. The best fit for the AM and PM values is shown

5. Results and Discussion

The SPATRAM data of spectral diffused solar radiation along the zenith direction are analyzed for the period 1st of April 2004 – 20th of June 2005. To obtain the SCD of the investigated species, the DOAS algorithms are applied in the 430-450 nm and 320-340 nm spectral windows where the strongest absorbers are NO$_2$ and O$_3$ respectively. The VCD of both NO$_2$ and O$_3$ are obtained through Eq. (7), where the AMF is calculated with the AMEFCO radiative transfer model [24]. AMEFCO is based on the Intensity Weighted Optical Path (IWOP) method and is a single-scattering model using ray tracing in a spherical two-dimensional atmosphere with optical paths integrated over individual shells. Light refraction is not included. In order to avoid bias due to the seasonal dependency of the vertical profile and hence in the AMF, different boundary condition are applied to the model with the aim to distinguish summertime and wintertime air masses. In order to take into account the intra-season difference in the AMF, a linear dependency of the AMF with seasons is assumed, being the values obtained for summer and winter interpolated and results utilized for the retrieval of VCD during the fall and spring seasons. Since SPATRAM carries out measurements continuously, the spectral data are obtained for unsystematic values of SZA. Due to the wavelength dependency of the AMF, together with the fact that the lowest error associated with the measurements are obtained for high values of SZA, the values of VCD for NO$_2$ and O$_3$ are calculated with a cubic spline interpolation of the data at 90° and 87° respectively, using at least four data points. This approach allows for the best estimation of the VCD values, since the interpolation function pass through all the data points. In addition, if one of the fitting points presents large variation with respect to the nearest ones, the point is not utilized by the spline algorithms, since the VCD time series are almost linear for small intervals of SZA. The errors associated with the presented results are in the range of 3-5% for the NO$_2$ VCD at 90° and 2-4% for the O$_3$ VCD at 87°. Values with larger errors, due to very low signal intensities or caused by the failure of the DOAS alignment algorithms, are rejected.

In Fig. 5(a), the NO$_2$ SCD values are plotted versus the SZA; the maximum values of NO$_2$ SCD for the morning period (AM) and for the afternoon period (PM) are obtained for a Solar

Zenith Angle of 93°. It has to be noted that the measurements can be obtained for angles greater than 90° (almost for 94°-95° of SZA), when the scattered light is very weak. To note that the PM values are higher than the AM values due to the photochemical activity of the nitrogen dioxide, as foreseen from the chemical reactions (3) and (5).

In Fig. 5(b), the O_3 SCD values are plotted versus the SZA in order to examine the different behavior, in terms of photochemical activity and diurnal variation, of O_3 respect NO_2. Whereas the maximum values of NO_2 SCD are obtained for the uppermost SZA (93°), for O_3 the upper limit of $(4.21 \pm 0.04) \times 10^{+19}$ molecules cm^{-2} for SZA of 87° is measured. In Fig. 5(b), also the weighted linear combination of the AMF calculated in the spectral range 320-340 nm (the spectral window utilized for the O_3 retrieval) is included in the plot. It has to be noted how the AMF overlie the O_3 SCD, allowing for the possibility to obtain the diurnal variation of O_3 in terms of vertical column applying Eq. (7)
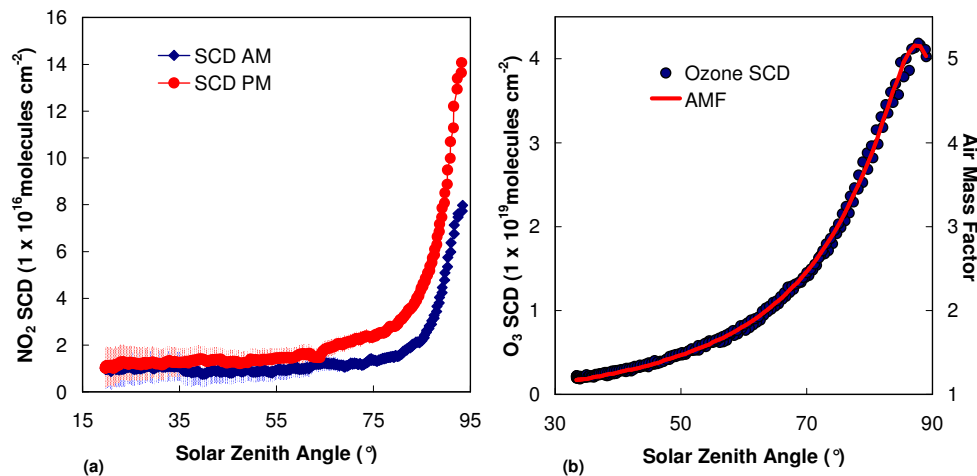
Fig. 5. (a) NO_2 SCD AM and PM values, obtained for the 29 July 2004, plotted versus the Solar Zenith Angle; (b) O_3 SCD AM and PM values, obtained for 3 April 2004, and calculated AMF, plotted versus the Solar Zenith Angle

Space-borne instruments and ground-based spectrometers capture major stratospheric features similarly. Although it is difficult to evaluate the accuracy of the NO_2 total column due to various problems such as the diurnal variation of NO_2 and the profile shape effect on the Air Mass Factor (AMF), the overall accuracy in areas of low tropospheric NO_2 is estimated to fall within the 5% to 20% interval [25].

Comparison of GOME NO_2 total content measurements with the simultaneous ground-based Vertical Column Density (VCD) observed at the CGE observatory during the first two months of activity of the SPATRAM equipment, are shown in Fig. 6. It can be noted that the GOME data are closer to the SPATRAM AM results due to the fact that the overpass of the ERS-2 satellite over Evora is around 11:30, when the photochemical process of NO_2 creation is just started. It is also possible to consider the positive seasonal trend of NO_2 VCD, reaching the higher value at the end of spring and the minimum lower values at the beginning of the spring season.
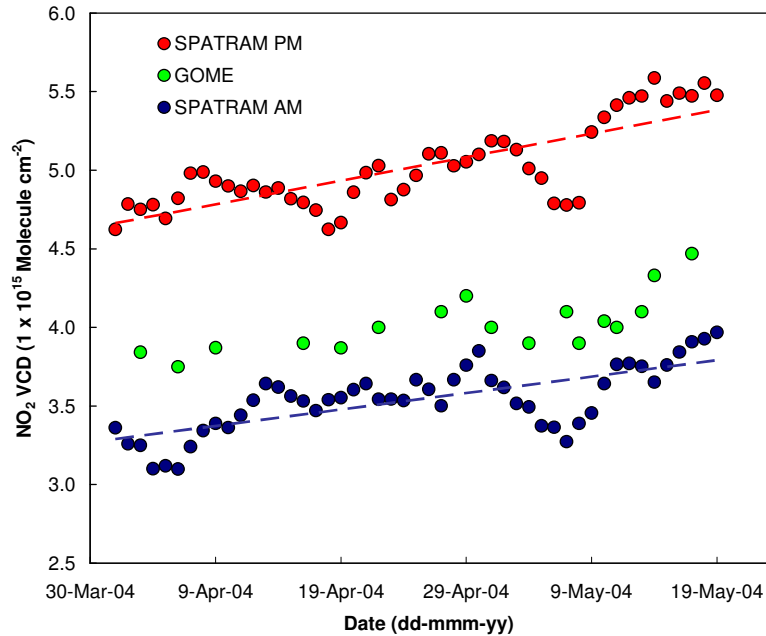
Fig. 6. NO$_2$ Vertical Column Density(VCD) at 90° of SZA (AM - sunrise and PM - sunset) obtained with SPATRAM and GOME results during the first 2 months of activity of the ground based equipment at the Evora station.

Figure 7 shows the NO$_2$ VCD values obtained with the ground based instrument and the SCIAMACHY spectrometer on board the ENVISAT satellite for the period November 2004 - June 2005.
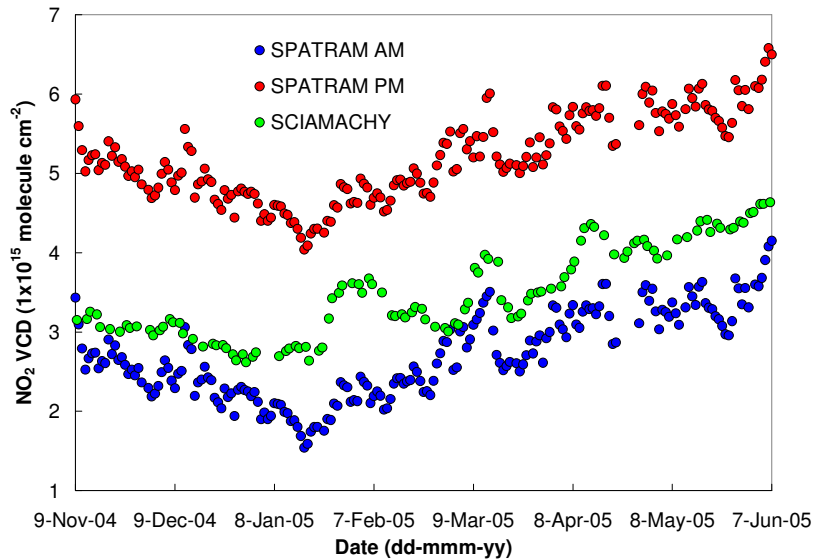

Fig. 7. Time series of the NO$_2$ Vertical Column Densities (VCD)obtained with the SPATRAM equipment installed at the Evora station at sunrise (AM) and sunset (PM) – SZA = 90°, and the NO$_2$ data from the SCIAMACHY spectrometer.

The two data sets are in good agreement and, due to the overpass of ENVISAT in the morning, the SCIAMACHY values almost overlay the AM SPATRAM data. The typical NO_2 seasonal cycle is more marked than in Fig. 6, ranging from the maximum value $(6.5 \pm 0.3) \times 10^{+15}$ molecules cm^{-2} for the sunset values (PM), during the summer season to the minimum of $(1.55 \pm 0.07) \times 10^{+15}$ molecules cm^{-2} for the sunrise value (AM), occurring in the winter season. It has also to be noted that both instruments identify the short term variations (with a period of about 30 days) in the NO_2.VCD.

The results obtained with SPATRAM for the O_3 Vertical Column content values during 2004 were compared with the corresponding data from TOMS and are displayed in Fig. 8. The O_3 seasonal cycle exhibits the maximum value of (433 ± 5) DU in the spring season and the minimum value of (284 ± 3) DU during the fall period, as expected. The O_3 seasonal cycle is also in agreement with other authors [26,27]. In this figure, note the good agreement between the two data sets and the concordance with the results reported by Mc Peters [15], by which the O_3 total column content provided by the TOMS instrument is about 1% higher than the ground-based measurements in the mid-northern latitude stations. Considering three seasons within the overall period of Fig. 9, spring (*AM*), summer (*JJA*) and fall (*SO*), the averages and standard deviations of TOMS O_3 and SPATRAM O_3 column contents for each season are found to be: 354 ± 26 DU, 315 ± 17 DU, 292 ± 15 DU for the TOMS O_3 column content values and 352 ± 26 DU, 313 ± 17 DU, 290 ± 15 DU for the SPATRAM O_3 column content values, being consistent with the values reported by Mc.Peters [15]. The huge variation of O_3 VCD during the spring season (the total column fluctuates from 430 to 275 DU during the first 20 days of April 2004) may be caused by two atmospheric dynamical processes: i) the air mass transport from the high latitudes with low O_3 concentration as a consequence of the NH polar vortex disappearance, at the end of the so-called "Ozone-Hole" period; ii) the adiabatic vertical displacement of isentropes [28–30]. Furthermore, the identification of a reasonable number of peaks of high and low O_3 Vertical Column content can also be associated with the winter/spring synoptic conditions typically occurring at the mid-northern latitudes, where transport of northern air masses occur during the passage of low pressure and frontal systems [31,32].
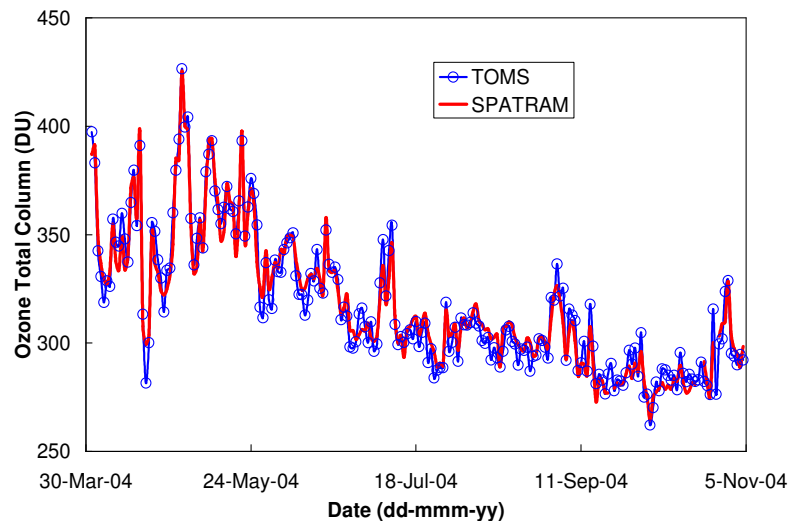

Fig. 8. Comparison of the seasonal variation of O_3 VCD at Evora Station with the seasonal variation reported by the TOMS instrument.

The O_3 data of Fig. 8 are represented in the scatter plot of Fig. 9, where SPATRAM vs TOMS VCD are shown, for a sample of 212 data points. The linear fit obtained ($O_{3\,SPATRAM} = 0.936 \times O_{3\,TOMS} + 20.107$) reveals a slight underestimation of SPATRAM with

respect to TOMS. However, the correlation coefficient obtained (R = 0.97) proves the good agreement between both data sets.
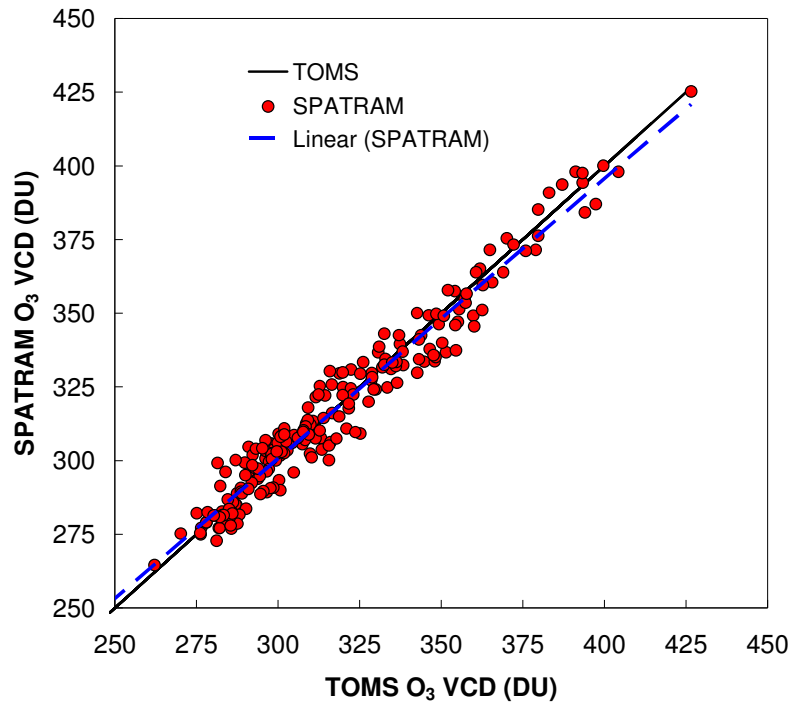

Fig. 9. Scatter plot of the SPATRAM vs TOMS O_3 vertical column, from October 2006 to June 2008. The number of data points for the SPATRAM O_3 values is n = 212. The linear fitting give the equation $O_{3\,SPATRAM} = 0.936 \times O_{3\,TOMS} + 20.107$ and the correlation's coefficient is R = 0.97.

6. Conclusions and future perspectives

The goal to develop, setup and install an automatic DOAS instrument at the Observatory of Evora, for the measurements of atmospheric tracers in unattended mode, was reached. A short description of the ground based equipment, in terms of optical and spectral features, is provided, underlining the conceptual effortlessness of the principle of measure. The differences with the previous version of the GASCOD spectrometer highlight innovations in the set up of this new instrument, the reliability of the entire equipment and of the spectral measurements. Furthermore, the possibility to manage the instrument via any internet connection allows for its installation also in very remote sites. The use of the Flux Index (FI) values for a first selection of the spectral data that can be utilized for the retrieval of the tracers is explained. The Flux index is also used in choosing the proper reference spectrum ($I_o(\lambda, \theta_{Min})$), analyzing the series of FI values and identifying a clear sky day where, at local noon, $I_o(\lambda, \theta_{Min})$ is obtained under optimal meteorological condition. The application of the DOAS algorithm for the determination of the background content of NO_2 and O_3 in the reference spectrum and the consequent assessment of the actual Slant Column Density (SCD) of the above mentioned compounds was also presented.

The typical diurnal variation, in terms of Slant Column Density SCD, of NO_2 and O_3 reveals the different behaviors of the two atmospheric compounds subject of this study.

Vertical columns contents of NO_2 for the period November 2004 - June 2005 and vertical column of O_3 for the period April - November 2004 are presented and discussed.

The seasonal cycle and the diurnal variations for the column values of NO_2 show a good agreement with both the photochemical theory of the NO_x family and the values observed by other authors in mid-latitude sites [33–36]. The NO_2 seasonal cycle presents the maximum value of $(6.5 \pm 0.3) \times 10^{+15}$ molecules cm^{-2} during the summer season, whilst the minimum of $(1.55 \pm 0.07) \times 10^{+15}$ molecules cm^{-2} is observed for the winter season. The comparisons of the results for NO_2 VCDs retrieved from the SPATRAM measurements with the GOME and SCIAMACHY products encourage continuing the comparison studies with ground-based reference instruments and satellite data aiming at the monitoring of atmospheric tracers.

The O_3 seasonal cycle exhibits the maximum value of (433 ± 5) DU in the spring season and the minimum value of (284 ± 3) DU during the fall period. The large O_3 Total Column daily variation during the first 20 days of April 2004 has to be related to the transport of air masses from the high latitudes as a consequence of the disappearance of the NH polar vortex. Furthermore, the identification of a reasonable number of peaks of high and low O_3 Vertical Column content can also be associated with the winter/spring synoptic conditions typically occurring at the mid-northern latitudes, where transport of northern air masses occur during the passage of low pressure and frontal systems. The comparison of the SPATRAM and TOMS results, reveals a slight underestimation of SPATRAM with respect to TOMS.. However, the correlation coefficient obtained (R = 0.97) proves good agreement between the two data sets.

This activity of comparison/validation of the satellite results could be enlarged as the SPATRAM is similar to other spectrometers installed at the climatic Station of Lampedusa (south of Italy), at the Ottavio Vittori Station over the Mt Cimone (Italy) and at the Bulgarian Atmospheric Station in Stara Zagora.

Acknowledgments